Journal of Applied Physics

Phonon transport at interfaces: Determining the correct modes of vibration

Cite as: J. Appl. Phys. **119**, 015101 (2016); https://doi.org/10.1063/1.4939207
Submitted: 01 October 2015 . Accepted: 17 December 2015 . Published Online: 04 January 2016

Kiarash Gordiz, and Asegun Henry

JOURNAL OF APPLIED PHYSICS **119**, 015101 (2016)

Phonon transport at interfaces: Determining the correct modes of vibration

Kiarash Gordiz[1] and Asegun Henry[1,2,a)]
[1]*George W. Woodruff School of Mechanical Engineering, Georgia Institute of Technology, Atlanta, Georgia 30332, USA*
[2]*School of Materials Science and Engineering, Georgia Institute of Technology, Atlanta, Georgia 30332, USA*

(Received 1 October 2015; accepted 17 December 2015; published online 4 January 2016)

For many decades, phonon transport at interfaces has been interpreted in terms of phonons impinging on an interface and subsequently transmitting a certain fraction of their energy into the other material. It has also been largely assumed that when one joins two bulk materials, interfacial phonon transport can be described in terms of the modes that exist in each material separately. However, a new formalism for calculating the modal contributions to thermal interface conductance with full inclusion of anharmonicity has been recently developed, which now offers a means for checking the validity of this assumption. Here, we examine the assumption of using the bulk materials' modes to describe the interfacial transport. The results indicate that when two materials are joined, a new set of vibrational modes are required to correctly describe the transport. As the modes are analyzed, certain classifications emerge and some of the most important modes are localized at the interface and can exhibit large conductance contributions that cannot be explained by the current physical picture based on transmission probability. © *2016 AIP Publishing LLC*.
[http://dx.doi.org/10.1063/1.4939207]

I. INTRODUCTION

The current and prevailing view point for describing phonon transport at interfaces is based on the phonon gas model (PGM), which treats phonons as gas particles that impinge on an interface. It is then believed that when a phonon reaches the interface, there is a certain probability that its energy will be transmitted, which is referred to as its transmission probability. It is also almost ubiquitously assumed that when two bulk materials are joined, the modes of each material are largely unchanged, and the transport at the interface can be described in terms of the modes that would exist in each bulk material separately. A study by Landry and McGaughey[1] suggested that such an approach exhibits agreement with the interface conductance calculated from non-equilibrium molecular dynamics (NEMD) simulations and independent lattice dynamics based approaches. However, although widely used,[2–7] these ideas have never actually been proven, i.e., by demonstrating excellent agreement with experiments, as has been done with first principles approaches to thermal conductivity.[8,9] Thus, it is important to consider alternative perspectives that might provide more accurate and complete descriptions of the physics.

Intuitively, based on the abrupt change in vibrational character, one might expect that non-propagating and possibly localized modes might exist at an interface. However, what has been lacking is an approach for identifying or studying such modes, and the ultimate goal would be to assess whether their role in interfacial transport is even important. Here, we discuss the recently developed interface conductance modal analysis (ICMA) method developed by Gordiz and Henry,[10] which naturally not only includes the crucial effect of anharmonicity but also allows one to examine the validity of the assumption that one can describe interfacial transport in terms of the bulk material's modes.

In essence, the ICMA formalism is based on performing a modal decomposition of the heat flow at an interface and then substituting the modal contributions into either an equilibrium molecular dynamics (EMD) or NEMD expression for thermal interface conductance (TIC). The key question then becomes: Which set of modes should one use in the heat flow decomposition to calculate physically meaningful contributions? This is important, because any mathematically complete set is guaranteed to return the same total heat flow. However, different choices might ascribe different amounts of the heat flow and contributions to TIC to different frequencies. This is critical because different spectral contributions might then lead to different temperature dependent TIC predictions when quantum effects on the heat capacity are accounted for (i.e., by applying approximate quantum corrections).[11,12] For example, if the TIC is dominated by low frequency modes, the temperature regime where it will decrease towards zero at low temperatures may be quite low, versus if it is dominated by higher frequency modes, the temperature regime where TIC will decrease towards zero at low temperatures may occur at somewhat higher temperatures.

Before addressing this question, we first review the ICMA formalism in Section II. (More details can be found in Ref. 10.) Then, in Section III, different modal basis sets will be investigated for two different interfaces by both EMD and wave-packet (WP) simulations to determine the correct basis set. The two structures examined are the interface of two lattice-matched mass-mismatched Lennard-Jones (LJ) solids

a)Author to whom correspondence should be addressed. Electronic mail: ase@gatech.edu

and the interface of two lattice-matched mass-mismatched solids described by Tersoff interatomic potential. Having defined the correct modal basis set, deeper understanding of the physics can be obtained by classifying the modes of vibration (Section IV) and analyzing the map of correlations (Section V). Finally, our conclusions are presented in Section VI.

II. ICMA FORMALISM

Consider forming an interface by bringing two systems A and B into contact, each having N_A and N_B atoms. We can use the lattice-dynamics (LD) formalism[13] to obtain the complete $3N = 3(N_A + N_B)$ eigen solutions to the equations of motion describing the vibrations of the system when all the interactions are considered to be harmonic. These eigen solutions allow us to write the atomic displacements and velocities as

$$\mathbf{x}_i = \sum_n \frac{1}{(Nm_i)^{1/2}} \mathbf{e}_{n,i} X_n, \tag{1}$$

$$\dot{\mathbf{x}}_i = \sum_n \frac{1}{(Nm_i)^{1/2}} \mathbf{e}_{n,i} \dot{X}_n, \tag{2}$$

where n is the index for the eigen mode; $\mathbf{x}_i$, $\dot{\mathbf{x}}_i$, and m_i are the displacement from equilibrium, velocity, and mass of atom i respectively; and $\mathbf{e}_{n,i}$ is the eigen vector for mode n assigning the direction and displacement magnitude of atom i. From the inverse of the operations in Eqs. (1) and (2), we can define the normal mode coordinates of position and velocity for mode n (X_n and $\dot{X}_n$) as

$$X_n = \sum_i \frac{m_i^{1/2}}{N^{1/2}} \mathbf{x}_i \cdot \mathbf{e}_{n,i}^*, \tag{3}$$

$$\dot{X}_n = \sum_i \frac{m_i^{1/2}}{N^{1/2}} \dot{\mathbf{x}}_i \cdot \mathbf{e}_{n,i}^*, \tag{4}$$

where i is the index for the atom in the system, and $*$ represents complex conjugate. A system of N atoms has a Hamiltonian given by

$$H = \sum_i^N \frac{\mathbf{p}_i^2}{2m_i} + \Phi(\mathbf{r}_1, \mathbf{r}_2, \ldots, \mathbf{r}_n), \tag{5}$$

where Φ is the total potential energy of the system, and the position and momentum of atom i are denoted by $\mathbf{r}_i$ and $\mathbf{p}_i$, respectively. From Eq. (5), the individual Hamiltonian for atom i can be written as

$$H_i = \frac{\mathbf{p}_i^2}{2m_i} + \Phi_i(\mathbf{r}_1, \mathbf{r}_2, \ldots, \mathbf{r}_n), \tag{6}$$

where Φ_i is the potential energy assigned to a single atom.[14,15] Using the above definition of the Hamiltonian for an individual atom, the energy exchanged between materials A and B at each instant of time can be written as

$$Q_{A\to B} = -\sum_{i\in A}\sum_{j\in B}\left\{\frac{\mathbf{p}_i}{m_i}\cdot\left(\frac{-\partial H_j}{\partial \mathbf{r}_i}\right) + \frac{\mathbf{p}_j}{m_j}\cdot\left(\frac{\partial H_i}{\partial \mathbf{r}_j}\right)\right\}, \tag{7}$$

which is a general equation that is valid for any interatomic potential, as long as it can be written as a sum of individual atom energies. For the case of having pairwise interactions between materials A and B, Eq. (7) is reduced to

$$Q_{A\to B} = -\frac{1}{2}\sum_{i\in A}\sum_{j\in B}\mathbf{f}_{ij}\cdot(\dot{\mathbf{x}}_i + \dot{\mathbf{x}}_j), \tag{8}$$

where $\mathbf{f}_{ij}$ is the pairwise exchanged force between atoms i and j in the two materials.[16–18] Having pairwise interactions, half of the interaction energy is naturally partitioned with atom i and the other half with atom j. Using Eq. (8) and fluctuation-dissipation theorem,[19] Domingues *et al.*[17] showed that the TIC is proportional to the correlation between the equilibrium heat flow fluctuations via

$$G = \frac{1}{Ak_BT^2}\int_0^\infty \langle Q_{A\to B}(t)\cdot Q_{A\to B}(0)\rangle dt, \tag{9}$$

where G is the TIC between materials A and B, A is the cross-sectional contact area, k_B is the Boltzmann constant, T is the equilibrium system temperature, and $\langle\cdots\rangle$ indicates the calculation of the autocorrelation function. For simplicity, we will use Q instead of $Q_{A\to B}$ for interfacial heat flow in the ensuing discussion.

It can be seen from Eq. (9) that if one can obtain the modal contributions to the interfacial heat flow such that at each instant the obtained modal contributions sum to the total Q

$$Q = \sum_n Q_n, \tag{10}$$

then G can be rewritten as

$$\begin{aligned} G &= \frac{1}{Ak_BT^2}\int\left\langle\sum_n Q_n(t)\cdot Q(0)\right\rangle dt \\ &= \sum_n \frac{1}{Ak_BT^2}\int\langle Q_n(t)\cdot Q(0)\rangle dt. \end{aligned} \tag{11}$$

This then yields the individual modal contributions to G as

$$G_n = \frac{1}{Ak_BT^2}\int\langle Q_n(t)\cdot Q(0)\rangle dt, \tag{12}$$

where

$$G = \sum_n G_n. \tag{13}$$

Furthermore, the modal heat flux definition in Eq. (10) allows us to substitute for both of the total heat fluxes in Eq. (9) leading to another definition for G as

$$\begin{aligned} G &= \frac{1}{Ak_BT^2}\int\left\langle\sum_n Q_n(t)\cdot\sum_{n'} Q_{n'}(t)\right\rangle dt \\ &= \sum_n\sum_{n'}\frac{1}{Ak_BT^2}\int\langle Q_n(t)\cdot Q_{n'}(0)\rangle dt, \end{aligned} \tag{14}$$

where individual contributions from pairs of modes equal to

$$G_{n,n'} = \frac{1}{Ak_BT^2}\int \langle Q_n(t)\cdot Q_{n'}(0)\rangle dt. \tag{15}$$

This definition represents the TIC as the summation of all the auto-correlations and cross-correlations between eigen mode pairs n and n' in the system ($G = \sum_{n,n'} G_{n,n'}$) and provides new insight into the degree to which each pair of modes interact and contribute to interface conductance. As a result, the ICMA method presented above contains more detail and can potentially lead to deeper insights into the physics of TIC.

The important step is then to determine Q_n, with the requirement of Eq. (10) (i.e., $Q = \sum_n Q_n$), which can be accomplished by replacing the atomic velocities in Eq. (7) with their modal definition in Eq. (2)

$$\begin{aligned} Q &= \sum_{i\in A}\sum_{j\in B}\left\{\left(\sum_n \frac{1}{(Nm_i)^{1/2}}\mathbf{e}_{n,i}\dot{X}_n\right)\cdot\left(\frac{\partial H_j}{\partial \mathbf{r}_i}\right) - \left(\sum_n \frac{1}{(Nm_j)^{1/2}}\mathbf{e}_{n,j}\dot{X}_n\right)\cdot\left(\frac{\partial H_i}{\partial \mathbf{r}_j}\right)\right\},\\ Q_n &= \frac{1}{N^{1/2}}\sum_{i\in A}\sum_{j\in B}\left\{\left(\frac{1}{(m_i)^{1/2}}\mathbf{e}_{n,i}\dot{X}_n\right)\cdot\left(\frac{\partial H_j}{\partial \mathbf{r}_i}\right) + \left(\frac{1}{(m_j)^{1/2}}\mathbf{e}_{n,j}\dot{X}_n\right)\cdot\left(\frac{-\partial H_i}{\partial \mathbf{r}_j}\right)\right\}. \end{aligned} \tag{16}$$

Equation (16) is general and it can be simplified for pairwise interactions to

$$Q_n = \sum_{i\in A}\sum_{j\in B}\frac{-\mathbf{f}_{ij}}{2}\cdot\left(\frac{1}{(Nm_i)^{1/2}}\mathbf{e}_{n,i}\dot{X}_n + \frac{1}{(Nm_j)^{1/2}}\mathbf{e}_{n,j}\dot{X}_n\right). \tag{17}$$

Equations (16) and (17) are the definitions of modal contributions to interfacial heat flow.

III. MODAL BASIS SETS

Towards finding the correct set of modes to be used in the heat flow decomposition, we have identified three potential options for the modal decomposition of the interfacial heat flow (Eqs. (16) and (17)). If we consider two bulk materials labeled A and B, respectively, when they are joined and form an interface, the three choices for describing the modes that contribute to heat flow through their interface are denoted by {A/B}, {A + B}, and {AB}. The basis set {A/B} corresponds to the modes associated with the bulk of either material A or B, where one performs a LD calculation for each individual bulk material. The modal basis set {A + B} corresponds to the addition of the eigen solutions for each separate bulk material, whereby one simply assigns polarization vectors equal to zero for the atoms on side B, for modes on side A, and vice versa. The third choice is then basis set {AB}, which corresponds to the modes obtained from a LD calculation for the entire structure, containing both materials A and B along with their interface. The basis set choices {A/B} and {A + B} are conceptually consistent with the current view of interface transport, since they correspond to the modes of the bulk material and for crystals are guaranteed to yield all propagating modes that have well-defined velocities. Using the bulk modes, which have well-defined velocities, is critical to the current paradigm, because the PGM description of TIC casts each mode's contribution as proportional to its velocity.[5,20] Thus, a non-propagating or localized mode's contribution is ill-defined in the current paradigm, and it is therefore of critical importance to determine if {A/B} and/or {A + B} can still be used to describe interfacial transport.

The correct basis set can be determined based on purely theoretical considerations, because it must reproduce the expected behavior in the harmonic limit (e.g., as T → 0K). As T → 0K, the atomic interactions approach that of a perfectly harmonic potential, which then leads to purely elastic interactions, whereby modes can only transfer their energy to other modes with the same frequency. In general, there could be modes on one side of the interface (denoted side A) that are above the maximum frequency that can be supported on side B, which we label as the heavier or weaker material with a lower maximum vibration frequency denoted by $\omega_{max,B}$. Modes with frequencies above $\omega_{max,B}$ on side A have no corresponding mode with the same frequency on side B to exchange energy through elastic interactions. Therefore, in the T → 0K limit, these modes cannot contribute to the TIC when anharmonic coupling is disabled. It is important to note that this effect is correctly reproduced by MD simulations, as the WP method shows that modes above $\omega_{max,B}$ have 0% transmission.[4,21–23] This behavior is also well understood and reproduced by other established methods, such as the AGF method, since the majority of implementations of the AGF method are based on an elastic scattering assumption.[3,6,7,24,25] Thus, by simply testing which basis sets show zero contributions to the TIC from modes above $\omega_{max,B}$ as T → 0K, we can determine which basis is correct.

Here, we studied a simple interface between lattice matched LJ face-centered cubic (FCC) solids. The LJ potential is defined based on the following formula:[26]

$$\Phi = 4\varepsilon\left[\left(\frac{\sigma}{r}\right)^{12} - \left(\frac{\sigma}{r}\right)^{6}\right], \tag{18}$$

where ε and σ are the energy and distance parameters and r is the distance between two interacting atoms. We select equal values of ε and σ for both materials A and B, which results in equal lattice constants for the two sides. An

acoustic mismatch exists at the interface because the mass of the atoms on side B are four times the mass of atoms on side A ($m_B = 4m_A$). Both sides have FCC lattice structures. In LJ systems, the simulations can be performed in LJ dimensionless units,[27] but to have the results correspond to a physically meaningful system, we chose LJ parameters in our simulations to be equal to that of argon ($\varepsilon = 1.67 \times 10^{-21}$J, $\sigma = 3.405$Å, and $m_A = 6.6 \times 10^{-26}$kg (Ref. 28)). Thus, side A represents solid argon (mass m) and side B represents a fictitiously heavier solid argon (mass $4m$) and by averaging an isobaric-isothermal simulation at zero pressure and T = 1 K, the lattice constant was calculated as 5.26Å.

A. EMD simulations

In our EMD simulations for the interface between LJ crystals, the system consists of 3 × 3 × 60 FCC unit cells (each side 30 unit cells long), which includes 2160 atoms and 6480 eigen modes. We confirmed that increasing the size of cross section does not change the features observed in the results, which is in agreement with other reports.[16,25] Initially, an equilibration period equal to 2 ns is performed. Then, modal heat flux contributions (Q_n) are recorded for 5 ns in the micro-canonical ensemble. The modal contributions to the heat flow, Q_n, are then used in post processing, which leads to the calculation of modal thermal conductance (G_n). A time step of 1 fs was chosen for the simulations, and ten independent ensembles were simulated to reduce the standard deviation in TIC below 5%.[29] The TIC accumulation function was then computed for all three basis sets according to the ICMA formalism[10] and is shown in Fig. 1. At a temperature of 1 K, only the {AB} basis set shows the qualitatively correct behavior as all of the contributions above $\omega_{max,B}$ decay to zero. Both the {A/B} and {A + B} basis sets, however, still attribute large portions of the TIC to frequencies that only exist in the bulk of side A and cannot transmit any energy to side B.

It should be noted that 0% transmission above $\omega_{max,B}$ was also observed for a perfectly smooth interface between two lattice matched diamond structured materials, modeled with the Tersoff potential,[30] using parameters for Si on both sides of the interface and Si with a 4× larger mass on the other. For this structure, we used EMD simulations to calculate the modal contributions to TIC. The system consists of 3 × 3 × 36 diamond unit cells (each side 18 unit cells long), which includes 2592 atoms and 7776 eigen modes of vibration. By averaging in an isobaric-isothermal simulation at zero pressure and T = 1 K, the lattice constant was calculated as 5.43Å. The temperature of the simulation is set to T = 1 K. Initially, an equilibration period of 5 ns under the NPT ensemble is performed. Then, modal heat flux contributions (Q_n) were recorded for 10 ns in the micro-canonical ensemble. The modal contributions to the heat flow, Q_n, are then used in post processing, which leads to the calculation of modal thermal conductance (G_n). A time step of 0.5 fs was chosen for the simulations, and ten independent ensembles were simulated to reduce the standard deviation in TIC below 5%. The accumulations have been calculated for different basis sets and are presented in Fig. 2. Again, by using the {AB} basis set, no contribution to the TIC from frequencies above $\omega_{B,\max}$ was observed, yet for the {A/B} and {A + B} bases, the frequency dependence is qualitatively incorrect. Since only the {AB} basis set yields the qualitatively correct behavior in both cases, our conclusion is that {AB} is the correct choice.

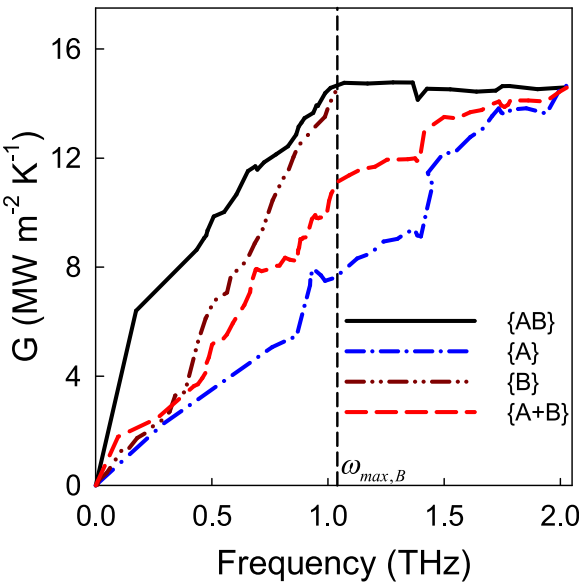

FIG. 1. Modal contributions to interface conductance at T = 1 K at the interface of two lattice matched, mass mismatched LJ solids calculated using different basis sets. {A/B} basis set can either express the modes on the bulk of side A or on the bulk of side B. The modal contributions from these two basis sets are shown in the figure using {A} and {B}, respectively. Since the {B} basis set is based on the heavier side of the interface, the maximum frequency in this basis set is $\omega_{max,B}$; therefore, the contributions by higher frequencies cannot be calculated using the {B} basis set.

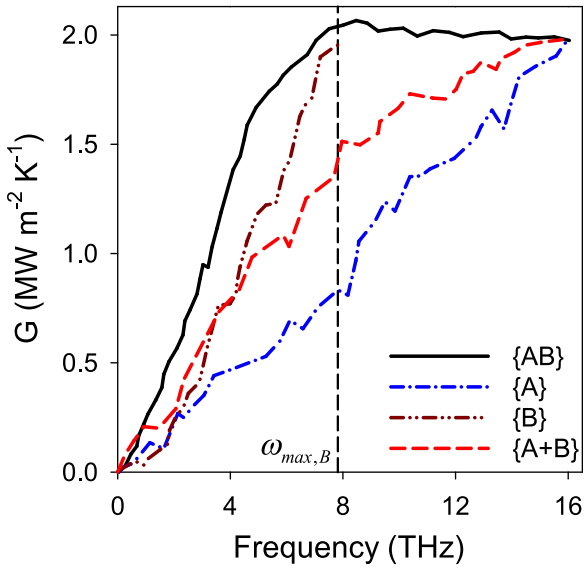

FIG. 2. Thermal interface conductance accumulation for different basis sets at the interface of a lattice matched, mass-mismatched silicon diamond structured system. Accumulation is calculated at a temperature of T = 1 K. {A/B} basis set can either express the modes on the bulk of side A or on the bulk of side B. The modal contributions from these two basis sets are shown in the figure using {A} and {B}, respectively. Since the {B} basis set is based on the heavier side of the interface, the maximum frequency in this basis set is $\omega_{max,B}$; therefore, the contributions by higher frequencies cannot be calculated using the {B} basis set.

B. Wave-packet simulations

To understand why {A/B} and {A + B} yield qualitatively incorrect behavior, a test was devised based on the WP method, whereby only a narrow range of frequencies with a single polarization is excited, and all other modes have zero amplitude which approximates T → 0K. The WP is launched towards the interface[22,23] from bulk of side A, and when it reaches the interface it elastically scatters, and a fraction of its energy is transmitted into modes with similar frequency on side B. We form the WP from the longitudinal polarization by displacing the atoms in the system according to Ref. 22

$$u_i = A_0 e_i(k_0) \exp\left[ik_0(z - z_0)\right] \exp\left[-\eta^2(z_1 - z_0)^2\right], \quad (19)$$

where the plane of the interface is perpendicular to the z-direction, A_0 is the amplitude of the wave packet, k_0 is the central wave vector for the WP, e_i (k_0) is the polarization vector for mode k_0 attributed to atom i, η is the spatial extent of the WP, and z_0 is the initial central location for the WP.[22]

For the WP simulations in this study, we set the parameters to be $A = 0.00001a_0$, $k_0 = 0.2\frac{2\pi}{a_0}$, $\eta = 50a_0$, and $z_0 = 150a_0$, where a_0 is the lattice constant for solid argon. Initial atomic velocities are assigned based on the differentiation of Eq. (19) with respect to time.[22] Initially, the WP has a certain amount of energy ($E_{init.}$), and when it reaches the interface, part of its energy is transmitted ($E_{trans.}$) and the remainder is reflected ($E_{refl.}$). The polarization of both the reflected and transmitted WPs can be different from the incident WP; however, both should have the same frequencies as the incident WP.[22] In the previous WP studies, the energy of different modes is studied and the transmission (τ) is computed from[23]

$$\tau = \frac{E_{trans.}}{E_{init.}}. \quad (20)$$

Using Eq. (17), the modal contributions to the interfacial heat flow are tracked in time for all three choices: {A/B}, {A + B}, and {AB}. For a correct basis set, the following two features should be observed: (1) Since the scattering event will be purely elastic, as the WP reaches the interface,

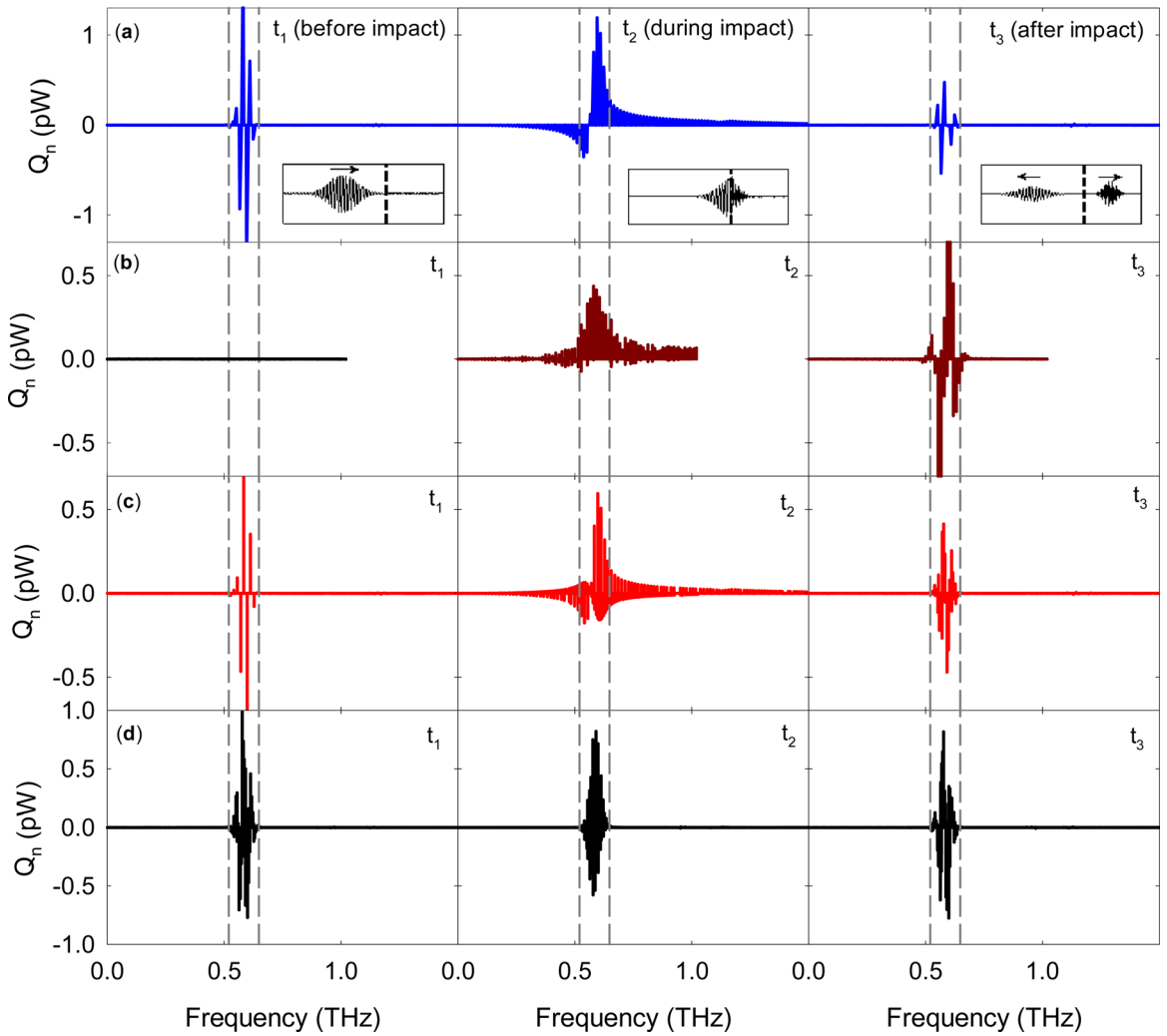

FIG. 3. Modal contributions to interfacial heat flow for the WP simulation at the interface of two lattice matched, mass mismatched LJ solids calculated using different basis sets of (a) {A}, (b) {B}, (c) {A + B}, and (d) {AB}. The data represent three different instants: before the impact (t_1), during the impact (t_2), and after the impact (t_3). The atomic displacement profiles at these three times are shown as insets in (a). The dashed lines show ($\Delta\omega$) the range of frequencies in the originally excited WP. Since the {B} basis set is based on the heavier side of the interface, the maximum frequency in this basis set is $\omega_{max,B} \approx 1.03$THz; therefore, the contributions by higher frequencies cannot be calculated using the {B} basis set.

we should only observe heat flow contributions Q_n associated with the original modes in the WP on side A or the modes in the transmitted WP on side B and (2) If we integrate Q_n in time, we should see that only the modes that participate in the incoming or outgoing WPs contribute to the energy transfer across the interface. Figure 3 shows that {A/B} and {A + B} do not exhibit these features, as they both show frequency broadening when the WP reaches the interface. This is unphysical because the frequency content of all the atomic motions before, during, and after the scattering event all lie within the same frequency range as the original WP. Therefore, the broadening exhibited by {A/B} and {A + B} is not representative of actual excitation of those frequencies. Instead, this broadening is a type of aliasing, since the modes in {A/B} and {A + B} do not contain information about the interface condition or bonding. Therefore, {A/B} and {A + B} ascribe contributions to modes that are not actually excited, which is why they assign large TIC contributions to modes with frequencies $> \omega_{max,B}$ as $T \rightarrow 0$ K(45% and 22%, respectively). However, only when the combined system {AB} is used are all of the theoretical requirements satisfied.

IV. CLASSIFICATION OF THE MODES OF VIBRATION

With the correct choice of modes now established, we turn our discussion to a deeper examination of the modes contained in the {AB} basis set. The interface itself acts as a compositional discontinuity that breaks the system's symmetry and changes the LD dynamical matrix in such a way that not all solutions can retain sinusoidally modulated eigen vectors for all of the atoms. Therefore, not all of the modes from the {AB} basis set correspond to propagating modes. Furthermore, since atoms near the interface have different dynamical matrix elements than the rest of the system, some of the eigen solutions become localized to the interfacial region (i.e., similar to localization of vibrational modes near defects).[31] Given that some degree of localization is to be expected, new mode classifications can emerge. One can then envision developing a mode classification scheme based on the degree to which modes are localized to a given portion of the system. For example, Eqs. (16) and (17) indicate that a mode can only contribute substantively to the heat flow, if it includes participation (e.g., significant eigen vectors) from atoms near the interface. Thus, a mode with zero eigen vectors for the atoms near the interface will by definition have zero contribution to the heat flow and therefore zero contribution to the TIC. Also, a mode that can extend through both sides of the interface and deeply into both materials has a greater likelihood of exhibiting longer correlation times, resulting in larger contributions to the TIC (see Eq. (9)). From this perspective, one might obtain new and interesting insights by classifying the modes in the {AB} basis set according to (1) the degree of delocalization into both materials, (2) the degree of localization in one material, (3) the degree of participation near the interface, or (4) the degree of localization near the interface.

We have tentatively classified the 3N solutions in the {AB} basis set into 4 distinct categories based on the region

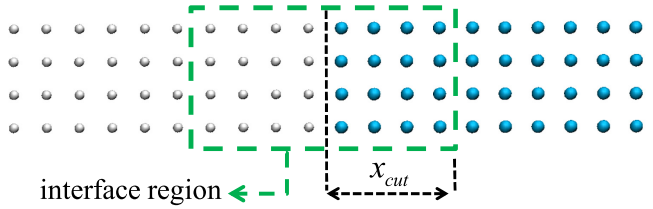

FIG. 4. Interface region. x_{cut} assigns the span of the interface region around the interface. For this study, the value of x_{cut} has been chosen equal to 10Å, which is equivalent to the LJ cut-off. For the diamond Si system, the cutoff was equal to two lattice constants.

where they are most localized: ⟨1⟩ extended modes, ⟨2⟩ partially extended modes, ⟨3⟩ isolated modes, and ⟨4⟩ interfacial modes. The criterion for classifying the modes in the LD calculation of the {AB} basis set is based on the answers to 2 questions motivated by inspection of Eqs. (16) and (17) in Section II, namely,

(1) Does the mode of vibration exhibit participation near the interface?
(2) Is the mode of vibration localized to any particular part of the system?

These two questions are motivated from the fact that if a mode does not exhibit significant participation in the interfacial region, it cannot exhibit a significant contribution to the interfacial heat flow or TIC. Conversely, if the majority of its vibrations are localized to the interfacial region, it can exhibit a significant contribution. Also, if a mode is delocalized across the interface and extends through both materials, it has a higher likelihood of exhibiting longer correlation times, which could lead to larger TIC contributions.

From LD calculations for the {AB} basis set, eigen vectors are defined for all the atoms and since we are interested in classifying eigen modes based on their vibrations with respect to the interface, we have defined four participation parameters (*PP*) to measure the magnitude of the eigen vectors for each atom in a given mode. The first *PP* sums the eigen vector magnitudes for eigen mode n in the entire structure (PP^n_{tot}). The second *PP* sums the eigen vector magnitudes for eigen mode n inside the interface region (PP^n_{int}), which is shown in Fig. 4. The third and fourth *PP* sums the eigen vector magnitudes for eigen mode n for side A, PP^n_A, and side B, PP^n_B, respectively. To define the interface region, we simply used a cutoff value, such that whenever the distance between an atom and the interface plane is less than x_{cut} (Fig. 4), the atom is considered inside the interface region. The cut off value for both the LJ and diamond Si systems was taken to be equal to two lattice constants. PP^n_{tot}, PP^n_{int}, PP^n_A, and PP^n_B for an eigen mode n are then defined as follows:

$$PP^n_{tot} = \sum_{i \in \text{entire system}} |\mathbf{e}_{n,i}|, \tag{21}$$

$$PP^n_{int} = \sum_{i \in \text{interface region}} |\mathbf{e}_{n,i}|, \tag{22}$$

$$PP^n_A = \sum_{i \in A} |\mathbf{e}_{n,i}|, \tag{23}$$

$$PP^n_B = \sum_{i \in B} |\mathbf{e}_{n,i}|. \tag{24}$$

The comparison of relative magnitudes for these four quantities is then used to classify each eigen mode n as one of the four types, based on answers to a series of questions. First, to answer the question: "*Is the mode present at the interface?*," we require PP^n_{int} to be a significant fraction of PP^n_{tot} (e.g., more than 0.1%), which leads to the requirement that $PP^n_{int}/PP^n_{tot} > 0.001$. To then answer the question: "*Is the majority of the vibration at the interface?*," we require that more than half of the vibrations be located within the interface region, which is mathematically expressed as the condition $PP^n_{int}/PP^n_{tot} > 0.5$. To then determine "*Is the mode localized to side A*" or "*Is the mode localized to side B?*," we require that one side of the interface exhibit at least 10 times larger portion of the vibrations (e.g., more than 90% of the vibration is on one side of the interface). This is then expressed mathematically as $PP^n_A/PP^n_B > 10$ to be localized on side A and $PP^n_B/PP^n_A > 10$ to be localized on side B. Thus, we then require $PP^n_A/PP^n_B \leq 10$ and $PP^n_B/PP^n_A \leq 10$ for delocalized modes. The four mode classifications are then defined by the following answers to the preceding questions and are summarized below using the corresponding mathematical statements:

Modes of type $\langle 1 \rangle$ are present at the interface, but the majority of the vibration is not at the interface, and they are delocalized into both materials.
Modes of type $\langle 2 \rangle$ are present at the interface, but the majority of the vibration is not at the interface, and they are localized on one side of the interface.
Modes of type $\langle 3 \rangle$ are not present at the interface.
Modes of type $\langle 4 \rangle$ have the majority of their vibration at the interface.

$$\begin{cases} PP^n_{int}/PP^n_{tot} > 0.001 \\ PP^n_{int}/PP^n_{tot} < 0.5 \\ PP^n_A/PP^n_B \leq 10 \\ PP^n_B/PP^n_A \leq 10 \end{cases}, \quad \text{mode } n \text{ is type } \langle 1 \rangle, \tag{25}$$

$$\begin{cases} PP^n_{int}/PP^n_{tot} \geq 0.001 \\ PP^n_{int}/PP^n_{tot} \leq 0.5 \\ PP^n_A/PP^n_B > 10 \end{cases}, \quad \text{mode } n \text{ is type } \langle 2 \rangle \text{ present in side A}, \tag{26}$$

$$\begin{cases} PP^n_{int}/PP^n_{tot} \geq 0.001 \\ PP^n_{int}/PP^n_{tot} \leq 0.5 \\ PP^n_B/PP^n_A > 10 \end{cases}, \quad \text{mode } n \text{ is type } \langle 2 \rangle \text{ present in side B}, \tag{27}$$

$$\text{mode } n \text{ is type } \langle 3 \rangle \text{ if it is not } \langle 1 \rangle, \langle 2 \rangle, \text{ or } \langle 4 \rangle, \tag{28}$$

$$PP^n_{int}/PP^n_{tot} > 0.5, \quad \text{mode } n \text{ is type } \langle 4 \rangle. \tag{29}$$

With this classification scheme, every eigen solution falls uniquely into one type and it is to be reiterated that the taxonomy introduced herein is preliminary. Additional studies are needed to determine the extent to which these mode definitions should be revised or expanded and whether or not these classifications serve as useful descriptors for the TIC.

Figure 5 shows examples of each of the four types of modes, and Fig. 6 shows their respective density of states. Extended modes (type $\langle 1 \rangle$) are delocalized over the entire system (Fig. 5(a)) and because both sides (A and B) vibrate at one frequency, their density of states has a sharp cutoff at $\omega_{max,B}$ (Fig. 6). Partially extended modes (type $\langle 2 \rangle$) vibrate on one side of the interface and only partially extend through to the other side (Fig. 5(b)). These modes comprise the majority of the eigen solutions (see Fig. 6). Isolated modes (type $\langle 3 \rangle$) exist on one side of the interface, but do not include participation near the interface (Fig. 5(c)). Interfacial modes (type $\langle 4 \rangle$) are localized/peaked near the interface (Fig. 5(d)) and they make up a small portion (0.3%) of the density of states, yet they play a significant role in the transport. The contributions to the TIC for each mode type are 42.87% (extended), 53.20% (partially extended), 0.55% (isolated), and 3.16% (interfacial). This indicates that, despite their low population, interfacial modes have the highest contribution on a per mode basis (10× higher than the average contribution per mode $G_{Total}/3\,N$).

To confirm that these mode classifications are not just a peculiar artifact of the LJ system, we have also performed the same calculations on the previously discussed Si interfaces modeled with the Tersoff potential, where the interaction parameters are the same for both sides, but the mass differs by 4×. LD calculations for such interfaces, as well as for interfaces where both the parameters and masses are different (i.e., corresponding to Si-Ge), again revealed the same 4 classifications of modes. Even more interestingly, when the modal contributions to TIC are calculated for these lattice-matched mass-mismatched Si interfaces at a higher temperature of $T = 400\,K$, a narrow band of interfacial modes between 12 and 13 THz, which only comprise 0.3% of the modes, are responsible for ~20% of the TIC (Fig. 7(a)). For these ICMA calculations, the simulation parameters are the same as those used to obtain the results shown in Fig. 2, except that the lattice constant at this temperature is equal to 5.54Å. The increase in conductance in the frequency range of 12–13 THz is so large that it leads one to question whether or not it can be considered anomalously high by comparison to the maximum conductance that can be obtained from modes described by the PGM. Although one could attempt to argue that the preceding observations may still be somewhat explainable by some modification of the PGM, the silicon diamond structured system exhibits individual conductance contributions that are so large that they cannot be predicted by the PGM at all. According to the Landauer formalism, the net heat flow (q) across the interface of two materials A and B is written as[20,32]

$$q = \sum_{p_A} \left[\frac{1}{V_A} \sum_{k_{x,A}=-k_{max}}^{k_{max}} \sum_{k_{y,A}=-k_{max}}^{k_{max}} \sum_{k_{z,A}=0}^{k_{max}} v_{z,A} \hbar\omega \tau_{AB} (f(\omega, T_A) - f(\omega, T_B)) \right], \tag{30}$$

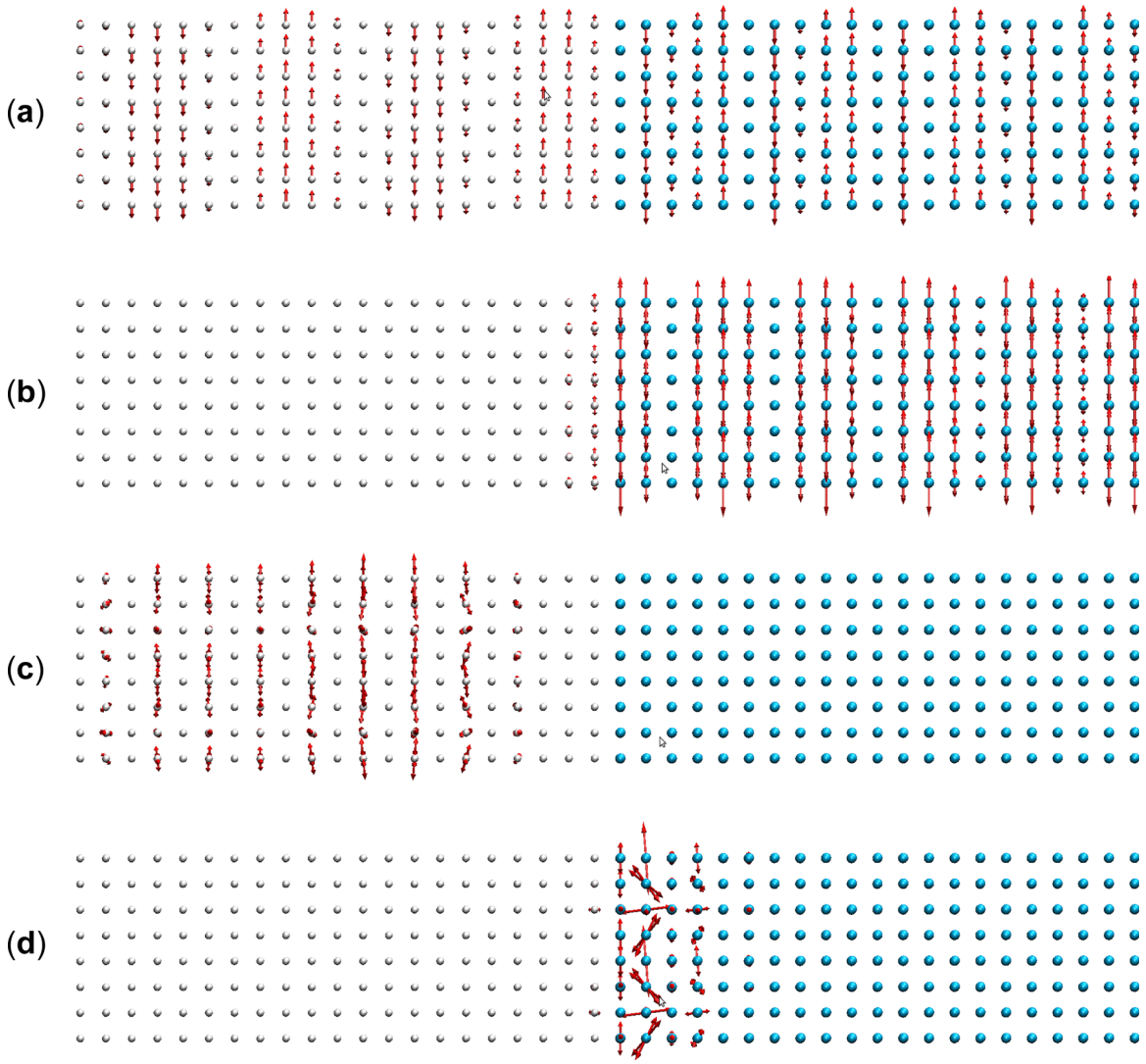

FIG. 5. Examples of the four classifications of eigen modes identified for the {AB} basis set for the interface of two lattice matched, mass mismatched LJ solids. Each panel shows eigen vector displacements for an example of each type of solution: (a) extended ⟨1⟩, (b) partially extended ⟨2⟩, (c) isolated ⟨3⟩, and (d) interfacial ⟨4⟩ modes. The frequencies of vibration for these for examples of eigen modes of vibration are 0.34 THz, 0.68 THz, 0.96 THz, and 0.47 THz, respectively.

where the summations are over different polarizations (p) and allowed wave vectors ($k_{x,y,z}$) in material A (i.e., modes with positive k_z and positive group velocities that are moving toward the interface and exist only on one side of the interface), V_A is the volume of side A, $v_{z,A}$ is the phonon velocity normal to the interface, $\hbar$ is the Planck's constant, ω is the frequency of vibration, τ is the transmission probability for the mode of vibration, and f is the Bose-Einstein distribution function. The definition of heat flow in Eq. (30) results in the following expression for conductance:[20]

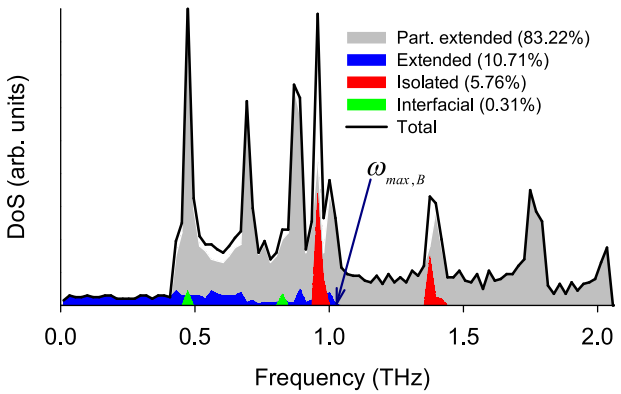

FIG. 6. Density of states and population (i.e., percentage of the total number of modes) for the four classifications of eigen modes identified for the {AB} basis set for the interface of two lattice matched, mass mismatched LJ solids.

$$G = \sum_{p_A} \left[\frac{1}{V_A} \sum_{k_{x,A}=-k_{max}}^{k_{max}} \sum_{k_{y,A}=-k_{max}}^{k_{max}} \sum_{k_{z,A}=0}^{k_{max}} v_{z,A} \hbar\omega \tau_{AB} \frac{df(\omega,T)}{dT} \right]. \tag{31}$$

To obtain the upper limit of modal contributions that can be obtained from the PGM, we used the classical high temperature limit for the mode heat capacity, such that Eq. (31) simplifies to

$$G = \sum_{p_A} \left[\frac{1}{V_A} \sum_{k_{x,A}=-k_{max}}^{k_{max}} \sum_{k_{y,A}=-k_{max}}^{k_{max}} \sum_{k_{z,A}=0}^{k_{max}} v_{z,A} \tau_{AB} k_B \right]. \tag{32}$$

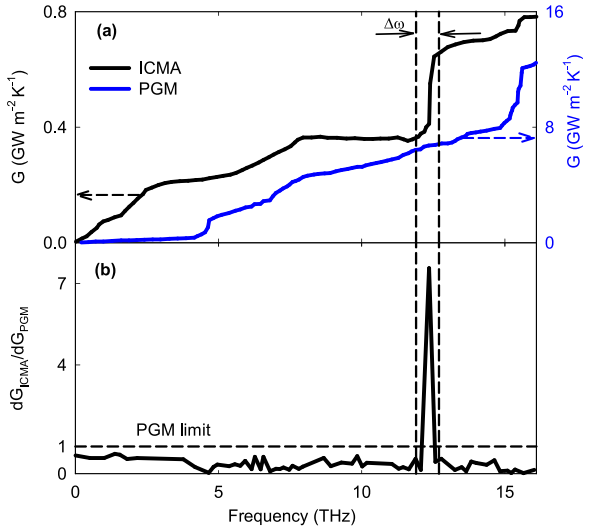

FIG. 7. Accumulation function for the thermal interface conductance at the interface of a lattice matched, mass-mismatched diamond structured (silicon) system at T = 400 K. (a) shows the comparison between the ICMA results and an upper limiting value associated with the PGM. (b) shows the ratio of the slope (rate of increase) of accumulation function calculated by ICMA to the maximum slope that can in any way be rationalized by the PGM. It is seen that the rate of increase in the frequency of range of $\Delta\omega$ exceeds the maximum PGM prediction, becoming larger than unity (PGM limit).

Equation (32) only utilizes the vibrational information of the left side of the interface. In an effort to compare to an upper limiting case, we can further assume that all of the left side vibrational modes can completely transfer their energy to the other side of the interface with a transmissivity of unity ($\tau = 1$). We can further assume that all modes are assigned the maximum velocity held by any mode in the system, namely, the speed of sound in silicon (8000m/s).[33] Under these upper limiting assumptions, the maximum conductance that a mode of vibration (n) can exhibit based on the PGM description is calculated by

$$G_{max,n} = \left(\frac{1}{V_A}\right) v_{z,A,\max} k_B, \tag{33}$$

which for silicon lattice $G_{max,n} = 7.18 \times 10^6 \mathrm{W/m^2K}$. Using this value as a reference, we calculated the accumulation function for the silicon diamond structured system using the calculated phonon DoS and assigning the maximum conductance possible from Eq. (33) for every mode as a conservative overestimation based on the PGM (Fig. 7(a)). The results show that the conductance contributions obtained from the ICMA method fall below the maximum PGM limit everywhere, except for the region between 12–13 THz, where there is a sharp increase. Figure 7(b) shows the ratio of the accumulation slopes obtained from the data in Fig. 7(a), which at each frequency represents the ratio of the increase in conductance predicted by ICMA to the maximum possible increase in conductance that could ever be explained by the PGM. This is an important new insight as it essentially suggests that there is no fundamental limit on the maximum conductance that can be observed at an interface, since the ICMA formalism shows that a given mode's conductance contribution is not bounded by the notion of 100% transmission as it is in the PGM. The unbounded nature of such a formalism arises from the fact that the final expression for TIC is proportional to an integral of an autocorrelation function. Other studies have shown that there may exist certain non-ergodic situations where the autocorrelation function does not fully decay, thereby giving rise to a divergent transport coefficient[34,35] and it is useful to recognize that the same possibility exists here.

Outside the frequency range of 12–13 THz, the values fall below unity, which does obey the PGM limit in Fig. 7(b). However, between 12 and 13 THz, the interfacial modes greatly exceed the PGM upper limit, which is a behavior that cannot be rationalized within the PGM paradigm. As a result, the ICMA formalism offers new possibilities for improving the conductance at interfaces, as it does not seem to be limited by the 100% transmission limit and therefore provides a new framework for thinking about interfacial heat flow engineering.

V. CORRELATION MAPPING

One of the other advantages of the ICMA method is that we can examine the extent of correlation/interaction between different modes through a 2D mapping of $G_{n,n'}$ correlations (Fig. 8) using Eqs. (16) and (17). To understand the modal interactions/correlations at the interface of two LJ solids in more detail, we calculated the 2D matrix of $G_{n,n'}$ correlations as shown in Fig. 8 as color maps and for different mode classifications as 3D correlation/interaction color maps in Figs. 9–14. Generally, the magnitude of auto-correlations ($n = n'$) is much larger than the cross-correlations ($n \neq n'$); therefore, removing auto-correlations from Fig. 8(a) presents a clearer view of the details of the cross-correlations as shown in Fig. 8(b). All of the $G_{n,n'}$ plots in Fig. 8 are symmetric about the diagonal, and examination of the plots leads one to notice interesting features that naturally emerge from the modal interactions. What is particularly interesting is that when analyzed with the {AB} basis set, features emerge at locations where mode character changes. For instance, in the LJ system, there is a region of minimal correlation in the frequency range of 0.4–1.0 THz. Here, 0.4 THz corresponds to the onset of localization (Fig. 6), where the first partially extended mode appears. Below 0.4 THz, all of the modes extend through the entire structure. Interestingly, 1.0 THz corresponds to $\omega_{max,B}$, whereby modes that extend into the bulk of the heavier side B cease to exist, since the bulk of side B cannot support higher frequency vibrations. The fact that distinct features in the mode-mode correlation are observed where the mode character changes is a further indication that the four classifications are meaningful. The majority of the modes present in the 0.4–1.0 THz frequency band are partially extended modes (type $\langle 2 \rangle$) that primarily exist on the heavier side of the interface (side B) and these partially extended modes exhibit much smaller correlations with other modes in the system, yet they contribute more than 50% of the TIC (see Fig. 1). Also, interfacial modes show the strongest correlation/interaction with the low frequency extended modes and higher frequency partially extended modes on the lighter side (side A). This leads us to

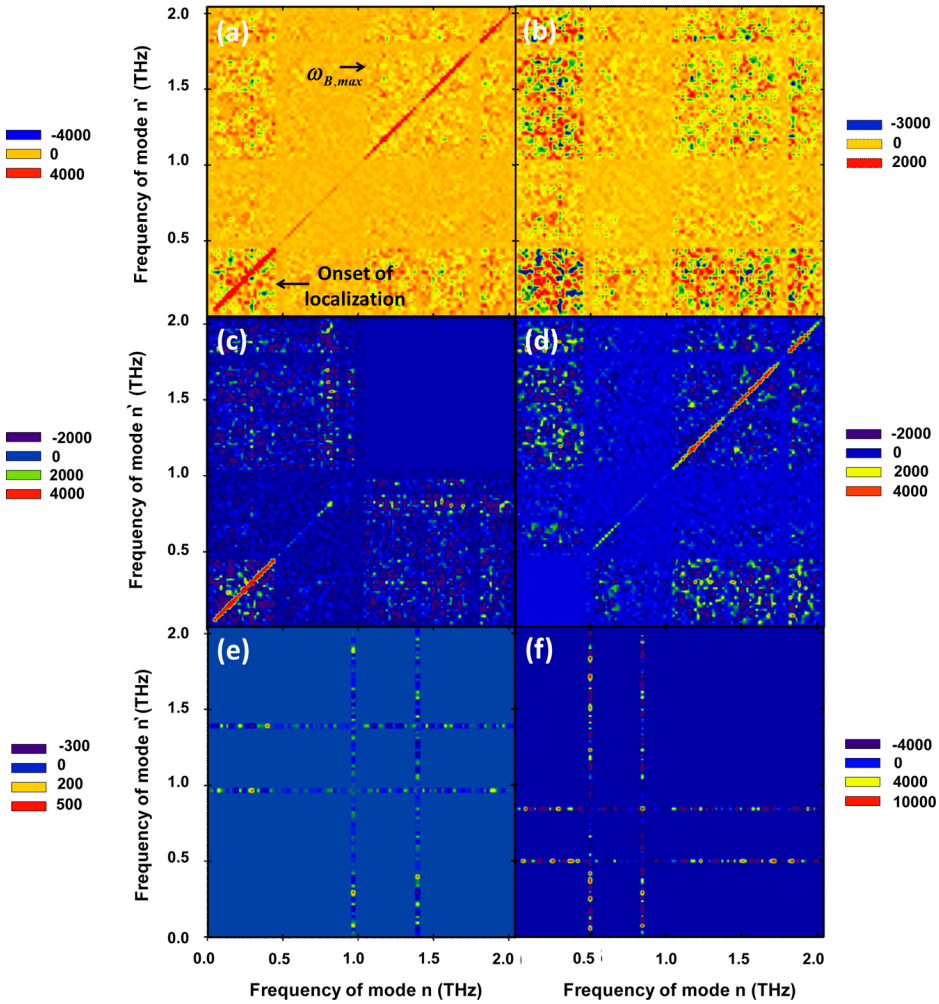

FIG. 8. Correlation contributions to thermal interface conductance between eigen modes n and n', $G_{n,n'}$ (W m^{-2} K^{-1}), at the interface of two lattice matched, mass mismatched LJ solids. The complete set of auto- and cross-correlations is in panel (a). Panel (b) shows only the cross-correlations after the auto-correlations have been artificially set to zero from the full set of correlations. (c)–(f) show correlations between the entire set of modes and the four classifications of vibrational modes (e.g., types ⟨1⟩–⟨4⟩), (c) shows ⟨1⟩ extended mode correlations, (d) shows ⟨2⟩ partially extended correlations, (e) shows ⟨3⟩ isolated mode correlations, and (f) shows ⟨4⟩ interfacial mode correlations.

conjecture that interfacial modes may help facilitate the transfer of the energy between low frequency extended modes and high frequency partially extended modes on the lighter side (side A) and vice versa. If true, these modes could serve as an important bridge for inelastic interactions, whereby modes with frequencies above $\omega_{B,\max}$ transfer their energy to interfacial modes at lower frequencies, which then transfer the energy into extended modes at even lower frequencies so it can propagate into the heavier side (side B). If true, this pathway provides a new physical picture for how interfacial transport can occur.

Another key feature captured by the {AB} basis set and not by {A/B} or {A + B} is that when two systems are

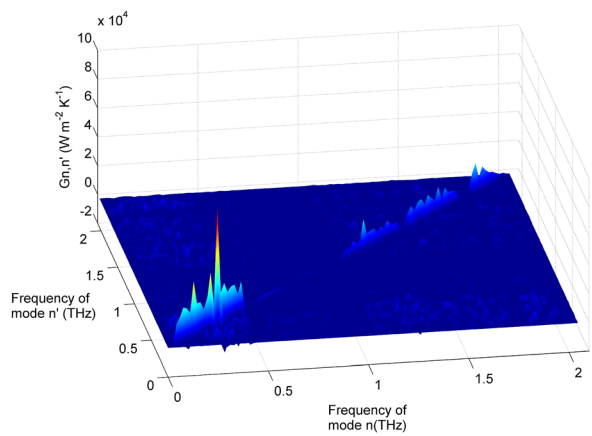

FIG. 9. Three-dimensional correlation contributions to thermal interface conductance between eigen modes n and n', $G_{n,n'}$, at the interface of two lattice matched, mass mismatched LJ solids. This plot shows the complete set of auto- and cross-correlations.

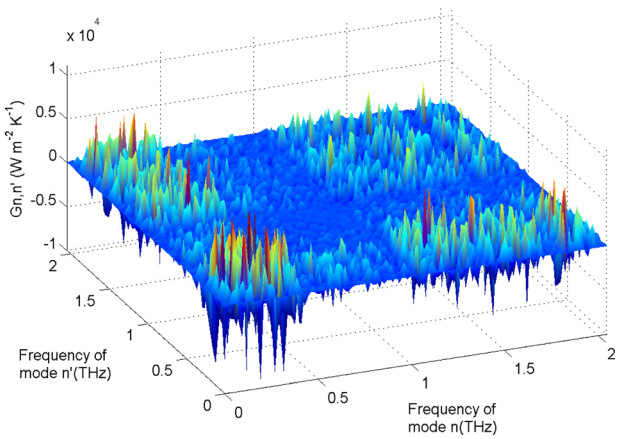

FIG. 10. Three-dimensional correlation contributions to thermal interface conductance between eigen modes n and n', $G_{n,n'}$, at the interface of two lattice matched, mass mismatched LJ solids. This plot shows only the cross-correlations after the auto-correlations have been artificially set to zero from the full set of correlations.

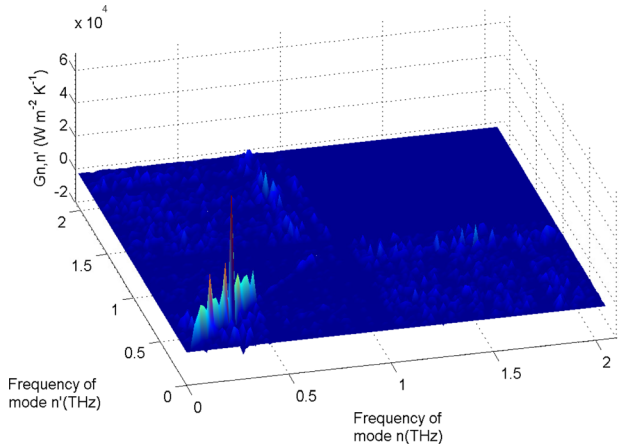

FIG. 11. Three-dimensional correlation contributions to thermal interface conductance between eigen modes n and n', $G_{n,n'}$, at the interface of two lattice matched, mass mismatched LJ solids. This plot shows correlations between the entire set of modes and the extended mode (type $\langle 1 \rangle$).

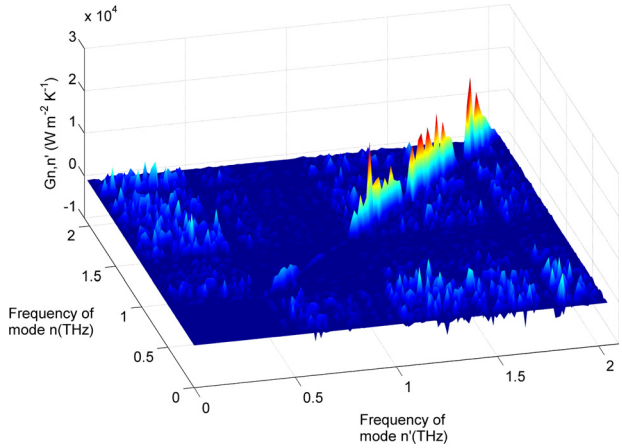

FIG. 12. Three-dimensional correlation contributions to thermal interface conductance between eigen modes n and n', $G_{n,n'}$, at the interface of two lattice matched, mass mismatched LJ solids. This plot shows correlations between the entire set of modes and the partially extended mode (type $\langle 2 \rangle$).

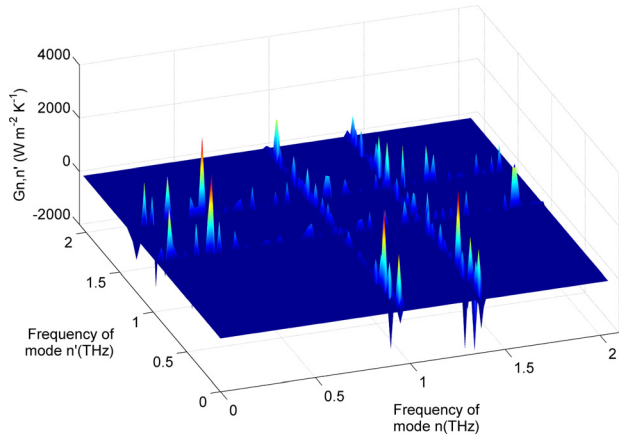

FIG. 13. Three-dimensional correlation contributions to thermal interface conductance between eigen modes n and n', $G_{n,n'}$, at the interface of two lattice matched, mass mismatched LJ solids. This plot shows correlations between the entire set of modes and the isolated mode (type $\langle 3 \rangle$).

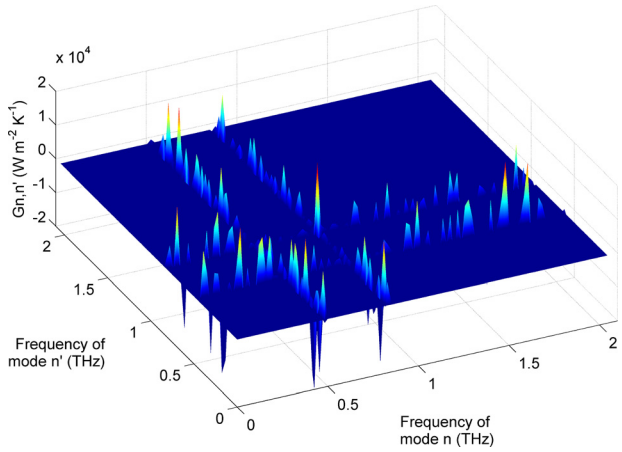

FIG. 14. Three-dimensional correlation contributions to thermal interface conductance between eigen modes n and n', $G_{n,n'}$, at the interface of two lattice matched, mass mismatched LJ solids. This plot shows correlations between the entire set of modes and the interfacial mode (type $\langle 4 \rangle$).

coupled together, the heavier atoms near the interface on side B can experience vibrations above $\omega_{max,B}$,[36,37] which is captured by the partially extended and localized modes near the interface. This feature is critical as it has been observed in actual MD simulations of interfaces,[36,37] but cannot be captured by the conventional modes contained in $\{A/B\}$ or $\{A+B\}$.

VI. CONCLUSION

The fact that one cannot use the same modes that existed in the native crystals to accurately understand what happens at an interface between dissimilar materials is a critical new insight. The fact that non-propagating localized modes can exist and exhibit the largest contributions to the TIC on a per mode basis further highlights the importance of thinking beyond the current PGM based view of interfacial transport, as previous models would be unable to account for the contributions of localized and/or non-propagating modes. The usage of the combined system's modal basis set $\{AB\}$ has far reaching implications, and the new ICMA based perspective provides a more general and complete physical picture that naturally includes all of the atomic level interface topography as well as anharmonicity to full order. Many additional studies to understand the effects of temperature, anharmonicity, interdiffusion, roughness, imperfections, dislocations, stress, changes in crystal structure, etc., are needed, but understanding which modes must be used serves as a critical step forward.

ACKNOWLEDGMENTS

We acknowledge useful discussions with Professor Michael Leamy.

[1]E. Landry and A. McGaughey, "Thermal boundary resistance predictions from molecular dynamics simulations and theoretical calculations," Phys. Rev. B **80**, 165304 (2009).
[2]W. Little, "The transport of heat between dissimilar solids at low temperatures," Can. J. Phys. **37**, 334–349 (1959).

[3]N. Mingo and L. Yang, "Phonon transport in nanowires coated with an amorphous material: An atomistic Green's function approach," Phys. Rev. B **68**, 245406 (2003).
[4]P. Schelling, S. Phillpot, and P. Keblinski, "Kapitza conductance and phonon scattering at grain boundaries by simulation," J. Appl. Phys. **95**, 6082–6091 (2004).
[5]E. T. Swartz and R. O. Pohl, "Thermal boundary resistance," Rev. Mod. Phys. **61**, 605 (1989).
[6]W. Zhang, T. Fisher, and N. Mingo, "The atomistic Green's function method: An efficient simulation approach for nanoscale phonon transport," Numer. Heat Trans., Part B **51**, 333–349 (2007).
[7]N. Mingo, *Thermal nanosystems and nanomaterials* (Springer, 2009), pp. 63–94.
[8]D. Broido, M. Malorny, G. Birner, N. Mingo, and D. Stewart, "Intrinsic lattice thermal conductivity of semiconductors from first principles," Appl. Phys. Lett. **91**, 231922 (2007).
[9]J. Garg, N. Bonini, B. Kozinsky, and N. Marzari, "Role of disorder and anharmonicity in the thermal conductivity of silicon-germanium alloys: A first-principles study," Phys. Rev. Lett. **106**, 045901 (2011).
[10]K. Gordiz and A. Henry, "A formalism for calculating the modal contributions to thermal interface conductance," New J. Phys. **17**, 103002 (2015).
[11]J. Turney, A. McGaughey, and C. Amon, "Assessing the applicability of quantum corrections to classical thermal conductivity predictions," Phys. Rev. B **79**, 224305 (2009).
[12]W. Lv and A. Henry, "Direct calculation of modal contributions to thermal conductivity via green-kubo modal analysis: Crystalline and amorphous silicon," New J. Phys. (to be published).
[13]M. T. Dove, *Introduction to Lattice Dynamics* (Cambridge University Press, 1993), Vol. 4.
[14]R. J. Hardy, "Energy-flux operator for a lattice," Phys. Rev. **132**, 168 (1963).
[15]A. S. Henry and G. Chen, "Spectral phonon transport properties of silicon based on molecular dynamics simulations and lattice dynamics," J. Comput. Theor. Nanosci. **5**, 141–152 (2008).
[16]Y. Chalopin, K. Esfarjani, A. Henry, S. Volz, and G. Chen, "Thermal interface conductance in Si/Ge superlattices by equilibrium molecular dynamics," Phys. Rev. B **85**, 195302 (2012).
[17]G. Domingues, S. Volz, K. Joulain, and J.-J. Greffet, "Heat transfer between two nanoparticles through near field interaction," Phys. Rev. Lett. **94**, 085901 (2005).
[18]Z.-Y. Ong and E. Pop, "Frequency and polarization dependence of thermal coupling between carbon nanotubes and SiO_2," J. Appl. Phys. **108**, 103502 (2010).
[19]R. Kubo, "The fluctuation-dissipation theorem," Rep. Prog. Phys. **29**, 255 (1966).
[20]G. Chen, *Nanoscale Energy Transport and Conversion: A Parallel Treatment of Electrons, Molecules, Phonons, and Photons* (Oxford University Press, USA, 2005).
[21]C. H. Baker, D. A. Jordan, and P. M. Norris, "Application of the wavelet transform to nanoscale thermal transport," Phys. Rev. B **86**, 104306 (2012).
[22]P. K. Schelling, S. R. Phillpot, and P. Keblinski, "Phonon wave-packet dynamics at semiconductor interfaces by molecular-dynamics simulation," Appl. Phys. Lett. **80**, 2484–2486 (2002).
[23]N. A. Roberts and D. Walker, "Phonon wave-packet simulations of Ar/Kr interfaces for thermal rectification," J. Appl. Phys. **108**, 123515 (2010).
[24]W. Zhang, N. Mingo, and T. Fisher, "Simulation of interfacial phonon transport in Si–Ge heterostructures using an atomistic Green's function method," J. Heat Transfer **129**, 483–491 (2007).
[25]Z. Tian, K. Esfarjani, and G. Chen, "Enhancing phonon transmission across a Si/Ge interface by atomic roughness: First-principles study with the Green's function method," Phys. Rev. B **86**, 235304 (2012).
[26]H. Rafii-Tabar, *Computational Physics of Carbon Nanotubes* (Cambridge University Press, 2008).
[27]A. Rajabpour and S. Volz, "Thermal boundary resistance from mode energy relaxation times: Case study of argon-like crystals by molecular dynamics," J. Appl. Phys. **108**, 094324 (2010).
[28]S. Sarkar and R. P. Selvam, "Molecular dynamics simulation of effective thermal conductivity and study of enhanced thermal transport mechanism in nanofluids," J. Appl. Phys. **102**, 074302 (2007).
[29]K. Gordiz, D. J. Singh, and A. Henry, "Ensemble averaging vs. time averaging in molecular dynamics simulations of thermal conductivity," J. Appl. Phys. **117**, 045104 (2015).
[30]J. Tersoff, "Modeling solid-state chemistry: Interatomic potentials for multicomponent systems," Phys. Rev. B **39**, 5566 (1989).
[31]A. M. Kosevich, "Localization of vibrations near extended defects," *The Crystal Lattice: Phonons, Solitons, Dislocations, Superlattices*, 2nd ed. (Wiley, 2006), Chap. 12, pp. 279–296.
[32]P. E. Hopkins, P. M. Norris, and J. C. Duda, "Anharmonic phonon interactions at interfaces and contributions to thermal boundary conductance," J. Heat Transfer **133**, 062401 (2011).
[33]J. V. Goicochea, M. Madrid, and C. Amon, "Thermal properties for bulk silicon based on the determination of relaxation times using molecular dynamics," J. Heat Transfer **132**, 012401 (2010).
[34]A. Henry and G. Chen, "Anomalous heat conduction in polyethylene chains: Theory and molecular dynamics simulations," Phys. Rev. B **79**, 144305 (2009).
[35]A. Henry and G. Chen, "High thermal conductivity of single polyethylene chains using molecular dynamics simulations," Phys. Rev. Lett. **101**, 235502 (2008).
[36]S. Shin, M. Kaviany, T. Desai, and R. Bonner, "Roles of atomic restructuring in interfacial phonon transport," Phys. Rev. B **82**, 081302 (2010).
[37]N. Yang *et al.*, "Thermal interface conductance between aluminum and silicon by molecular dynamics simulations," J. Comput. Theor. Nanosci **12**, 168–174 (2015).